International Journal of Materials Science and Applications
2015; 4(4): 246-255
Published online June 29, 2015 (http://www.sciencepublishinggroup.com/j/ijmsa)
doi: 10.11648/j.ijmsa.20150404.14
ISSN: 2327-2635 (Print); ISSN: 2327-2643 (Online)

Simulated Sunlight Induced the Degradation of Rhodamine B Over Graphene Oxide-Based Ag_3PO_4@AgCl

Mahgoub Ibrahim Shinger[1, 2], Ahmed Mahmoud Idris[1], Dong Dong Qin[1], Hind Baballa[1], Duoliang Shan[1], Xiaoquan Lu[1, *]

[1]Key Laboratory of Bioelectrochemistry & Environmental Analysis of Gansu Province, College of Chemistry & Chemical Engineering, Northwest Normal University, Lanzhou, China
[2]Chemistry Department, Faculty of Science, International University of Africa, Khartoum, Sudan

Email address:

shinger1977@yahoo.com (M. I. Shinger), ahmedwadmahmoud@yahoo.com (A. M. Idris), 395148255@qq.com (Dong Dong Qin), hindfnc@hotmail.com (H. Baballa), shandouliang@126.com (Duoliang Shan), luxq@nwnu.edu.cn (Xiaoquan Lu)

To cite this article:

Mahgoub Ibrahim Shinger, Ahmed Mahmoud Idris, Dong Dong Qin, Hind Baballa, Duoliang Shan, Xiaoquan Lu. Simulated Sunlight Induced the Degradation of Rhodamine B Over Graphene Oxide-Based Ag_3PO_4@AgCl. *International Journal of Materials Science and Applications*. Vol. 4, No. 4, 2015, pp. 246-255. doi: 10.11648/j.ijmsa.20150404.14

Abstract: A facile, environmentally friendly and economical in-situ ion-exchange method was successfully fabricated graphene oxide-based Ag_3PO_4@AgCl photocatalyst to promote the photocatalytic activity of Ag_3PO_4@AgCl. The as synthesized GO-Ag_3PO_4@AgCl composite was characterized by Fourier transform infrared (FTIR), X-ray diffraction (XRD), UV-vis diffuse reflectance spectroscopy and photoluminescence (PL). The morphology and the structure of the synthesized photocatalyst were characterized by field-emission scanning electron microscopy (SEM) and transmitter electron microscopy (TEM). The elements detection and the chemical state of the sample were investigated by X-ray photoelectron spectroscopy (XPS) analysis. GO-Ag_3PO_4@AgCl exhibited higher photocatalytic activity over Ag_3PO_4@AgCl and Ag_3PO_4 for the degradation of Rhodamine B (RhB) under simulated sunlight, and the highest photocatalytic activity was obtained by GO-Ag_3PO_4@AgCl photocatalyst with Cl/P ratio of 0.5. The quenching study using different scavengers investigated that the photogenerated holes (h^+) and superoxide radicals ($^{\bullet}O_2^-$) played a key role in the degradation of RhB. The kinetic study revealed that the degradation of RhB over GO-Ag_3PO_4@AgCl-0.5 under simulated sunlight followed the first-order kinetics.

Keywords: GO, Ag_3PO_4, AgCl, RhB and Simulated Sunlight Irradiation

1. Introduction

Photocatalysts as a new branch used as organic pollutant removal from wastewater have attracted considerable attention because of their potential applications for removal and degradation of organic dyes which falls as the largest group of water pollutants for their toxicity and carcinogenicity [1-3]. Recently Silver orthophosphate Ag_3PO_4 has been reported as a new visible light–driven photocatalyst with high photocatalytic performance for the oxygen evaluation from water and the photodecomposition of organic dyes under visible light irradiation [4-7]. But, Ag_3PO_4 has disadvantages, such as high cost of the starting material $AgNO_3$, and decomposing to weakly active Ag during the photocatalytic reaction process. Moreover, the irregular polyhedral microstructure of Ag_3PO_4 has poor dispersity/stability due to its slight solubility in aqueous solution [8]. As a result, more attention has been paid to investigate new Ag_3PO_4 photocatalyst systems with good structural, catalytic activity and stability. Thus, many studies have been synthesized Ag_3PO_4-based composites including Ag/Ag_3PO_4 [9], TiO_2/Ag_3PO_4 [10], Ag_3PO_4/ZnO [11] and SnO_2/Ag_3PO_4 [12]. In addition, the epitaxial growth of an AgX (X = Cl, Br and I) on the surface of Ag_3PO_4 could greatly enhance the chemical stability and activity of Ag_3PO_4 [13]. Recently, graphene oxide (GO) has become an ideal support for the photocatalysts, because of possessing two dimensional structures and large specific surface area may tailor the size and morphology of photocatalysts. Therefore, the cost for the synthesis of Ag_3PO_4-based photocatalysts can be greatly reduced. Moreover GO has conductive properties that give it excellent mobility of charge carriers, and high chemical and thermal stability [14-17]. Therefore, it is expected that the fabrication of graphene with Ag_3PO_4-based photocatalysts can greatly

improve its photocatalytic activity and stability. Recently, many groups have reported graphene-based Ag_3PO_4 photocatalysts with enhanced photocatalytic activity, such as GO-Ag_3PO_4 [18,19] and GO-Ag_3PO_4/Ag [20,21]. Therefore, the combination of graphene oxide, Ag_3PO_4 and AgCl may be regarded as a good photocatalytic system for achieving enhanced photocatalytic activity and stability.

According to our knowledge, till now, very few studies have reported the synthesis of Ag_3PO_4@AgCl due to the wide band gap of AgCl (3.2 eV), and no previous studies regarding the photocatalytic activity of GO-Ag_3PO_4@AgCl under simulated sunlight have been reported. In this study we synthesized graphene-based Ag_3PO_4@AgCl composite with enhanced photocatalytic activity via a simple in-situ ion-exchange method. Furthermore, we demonstrated that GO-based Ag_3PO_4@AgCl exhibited the enhancement of the photocatalytic degradation of Rhodamine B (RhB) over Ag_3PO_4@AgCl composite under simulated sunlight. In addition, prominently enhanced photocatalytic activity was carried out by comparing with Ag_3PO_4@AgCl in the present study. Moreover, the effect of mass ratios of AgCl in the GO-Ag_3PO_4@AgCl composites on the photocatalytic activity was also investigated comparatively.

2. Experimental

2.1. Materials

Chemicals used in this study all were of analytical grade used as reserved without further purification.

2.2. Synthesis of Graphene

Using modified Hummers method graphene oxide was prepared from natural graphite [22]. In a typical synthesis, 2.5 g of $K_2S_2O_8$ was added to 2.5 g of P_2O_8 in a round bottom flask and dissolved by12 ml of concentrated H_2SO_4 under stirring, followed by addition of 1 g of graphite and stirred for 30 min. Then the temperature was elevated to 80 ^oC and the reactants were kept on it to 4 h. After that cooled at room temperature and washed with distilled water several time until the pH of the solution reached 7. Then centrifuged and the precipitate was dried under vacuum at 60 ^oC for 24 h. Afterwards, 1 g of the dried precipitate was added to 36 ml of concentrated H_2SO_4 that was precooled to 0 ^oC and then stirred for 30 min for homogenization. Then, 5 g of $KMnO_4$ was slowly added to the contents and the temperature kept at less than 10 ^oC under stirring for 30 min. Then the temperature was slowly increased to 35 ^oC and left to react overnight. 350 ml of distilled water was added to the mixture followed by the addition of 5 ml of 30% H_2O_2 (the color changed to bright yellow) and stirred for 30 min. The obtained GO was washed by 5% HCl to remove metal ions followed by washing with distilled water several times until the pH of the solution reached 7. The obtained GO was then suspended in distilled water and ultrasonicated for 2 h, then centrifuged at 1100 r/min for 25 min, and the supernatant was removed and the GO was dried under vacuum at 60 ^oC for 24 h.

2.3. Synthesis of GO-Ag_3PO_4@AgCl

GO-Ag_3PO_4@AgCl was prepared by an in situ-ion exchange method. To 50 mg of GO suspended in 50 ml H_2O and stirred for 6h, 2.4 g/20 ml of $AgNO_3$ was added and stirred under dark condition for 12 h. Afterward, 1.152 g/20 ml of Na_2HPO_4 was added dropwise and the mixture kept stirred for 1 h followed by the dropwise addition of 20 ml of NaCl with Cl/P molar ratio of 0.3. Then the mixture was stirred for 6 h under the same condition. GO-Ag_3PO_4@AgCl particles were obtained by filtering of the precipitate followed by drying under vacuum at 60 ^oC for 24 h. Varying the amount of AgCl by the addition of NaCl with Cl/P molar ratio of 0.3, 0.5 and 0.7, different GO-Ag_3PO_4@AgCl photocatalysts were prepared, and defined as GO-Ag_3PO_4@AgCl-0.3, GO-Ag3PO4@AgCl-0.5 and GO-Ag_3PO_4@AgCl-0.7 respectively. For the comparison, using the same method different photocatalysts were prepared, Ag_3PO_4@AgCl was fabricated without the use of GO and pure Ag_3PO_4 was also synthesized without the use of any of GO and NaCl.

2.4. Material Characterization

Characterization of the Photocatalysts. X-ray diffraction (XRD) measurements were carried out at room temperature using a BRUKER D8 ADVANCE X-ray powder diffractometer with Cu-Kα radiation (λ = 1.5406˚A) in the 2θ range of 10 ^oC to 80 ^oC. The morphology and the composition were characterized using Scanning electron microscope (SEM) and a JSM-7001F (JEOL) transmission electron microscope (TEM). The UV-visible diffuse reflectance spectra were obtained by a Shimadzu UV2450 spectrophotometer. The Fourier transform infrared (FTIR) spectra of the samples were recorded on a Bruker Vertex 70 FT-IR spectrophotometer using the KBr method. The photoluminescence (PL) were measured at room temperature on a Varian Cary Eclipse fluorescence spectrophotometer with the excitation wavelength at 320 nm. Detection of the elements and chemical state of the sample were investigated by X-ray photoelectron spectroscopy (XPS) analysis.

2.5. Evaluation of Photocatalytic Activity

The study of the photocatalytic activity of the synthesized photocatalysts was carried out using RhB solution at room temperature. Briefly, 25 mg of the as prepared photocatalyst was mixed with 50 ml of RhB (0.005g/L) then sonicated for 10 min followed by stirring in dark condition for 30 min to establish adsorption-desorption equilibrium. Afterwards, the mixture was irradiated with simulated sunlight using a 350 W Xe lamp as light source. During the illumination, 3 ml aliquots were collected at a given time interval, then centrifuged to remove the photocatalyst. The concentration of RhB solution was determined by UV-visible spectrophotometer at 553 nm [23].

In order to detect the active species during the photocatalytic reaction, p-benzoquinone (BZQ), disodium ethylenediaminetetraacetate (Na_2-EDTA) and tert-butanol were added in to the RhB solution dispersed with the

GO-Ag_3PO_3@AgCl-0.5 to capture superoxide radical ($^{\bullet}O_2^-$), holes (h^+) and hydroxide radical ($^{\bullet}OH$), respectively, followed by the photocatalytic activity test.

3. Results and Discussion

3.1. FT-IR Analysis

In order to confirm the fabrication of Ag_3PO_4 and AgCl with GO sheets in GO-Ag_3PO_4@AgCl-0.5 photocatalyst, their FT-IR together with that of Ag_3PO_4@AgCl, Ag_3PO_4 and GO sheets are measured [Figure 1(A)]. The spectrum of GO sheets is included peak at 3420 cm^{-1} which attributed to the stretching vibration mode of $^-$OH, the stretching vibration band of the C=O carbonyl is appeared at about 1715 cm^{-1} (attributed to COOH groups), the peak at about 1640 cm^{-1} is attributed to the binding vibration of $^-$OH, at 1390 cm^{-1} the peak of the tertiary C-OH stretching vibration is appeared, and the broad peak band at around 1140 cm^{-1} is due to the absorption of the vibration band of epoxy and alkoxy groups [24,25]. For the spectrum of Ag_3PO_4, the peaks at 3420 and 1650 cm^{-1} are corresponded to the $^-$OH stretching and binding vibrations of physically absorbed H_2O molecules respectively. The peak at about 550 cm^{-1} is related to the O=P-O bending vibration, the peaks at about 850 and 995 cm^{-1} are attributed to the symmetric and asymmetric stretching vibrations of P-O-P rings respectively. At 1385 cm^{-1} the stretching vibration peak of P=O is observed [25]. In the spectrum of GO-Ag_3PO_4@AgCl-0.5 and Ag_3PO_4@AgCl composites, the characteristic bands for Ag_3PO_4 still remain, but the peak which attributed to the stretching vibration of the P–O–P group is shifted to 1017 and 1010 cm^{-1} in the spectrums of GO-Ag_3PO_4@AgCl-0.5 and Ag_3PO_4@AgCl respectively compared with that of Ag_3PO_4 spectrum (995 cm^{-1}). Nevertheless, the band intensity at 1385 cm^{-1} is became weakened. Moreover, a new absorption band is appeared at 1550 cm^{-1}, which is attributed to the skeletal vibration of the graphene sheets [26], proving the presence of GO in the spectrum of GO-Ag_3PO_4@AgCl-0.5 composites, suggesting the formation of GO-Ag_3PO_4@AgCl-0.5 from the interaction between GO, Ag_3PO_4 and AgCl.

3.2. XRD Analysis

The crystallographic structures of the as-obtained products are determined by X-ray diffraction (XRD) measurements. Ag_3PO_4 is a body-centered cubic structure, consists of isolated and regular PO_4 tetrahedral (P–O distance of ~1.539 Å) to form a body-centered cubic lattice, and six Ag^+ ions are distributed among 12 sites of the two-fold symmetry [27]. As shown in Figure 1(B), the XRD patterns of the as-synthesized composites show that all patterns marked with solid rhombus are matched very well with the standard data of Ag_3PO_4 (JCPDS No. 06-0505), which is consistent with the previous study [28]. For the pattern of GO-Ag_3PO_4@AgCl-0.5 and Ag_3PO_4@AgCl, besides the peaks of Ag_3PO_4, the diffraction peaks of AgCl at 2 theta = 27.9°, 32.3°, 46.4° 67.4° and 76.78° which are corresponding to the (111), (200), (220), (400) and (420) planes are also detected [29], confirming that AgCl is formed on the Ag_3PO_4 surface after the reaction with NaCl. However, no diffraction peak of graphene is observed in the XRD pattern of GO-Ag_3PO_4@AgCl-0.5, which may be due to the low diffraction intensity of the GO in the sample [30] or may be due to the destruction of the regular stack of graphene sheets by the assembly of Ag_3PO_4 nanoparticles [31].

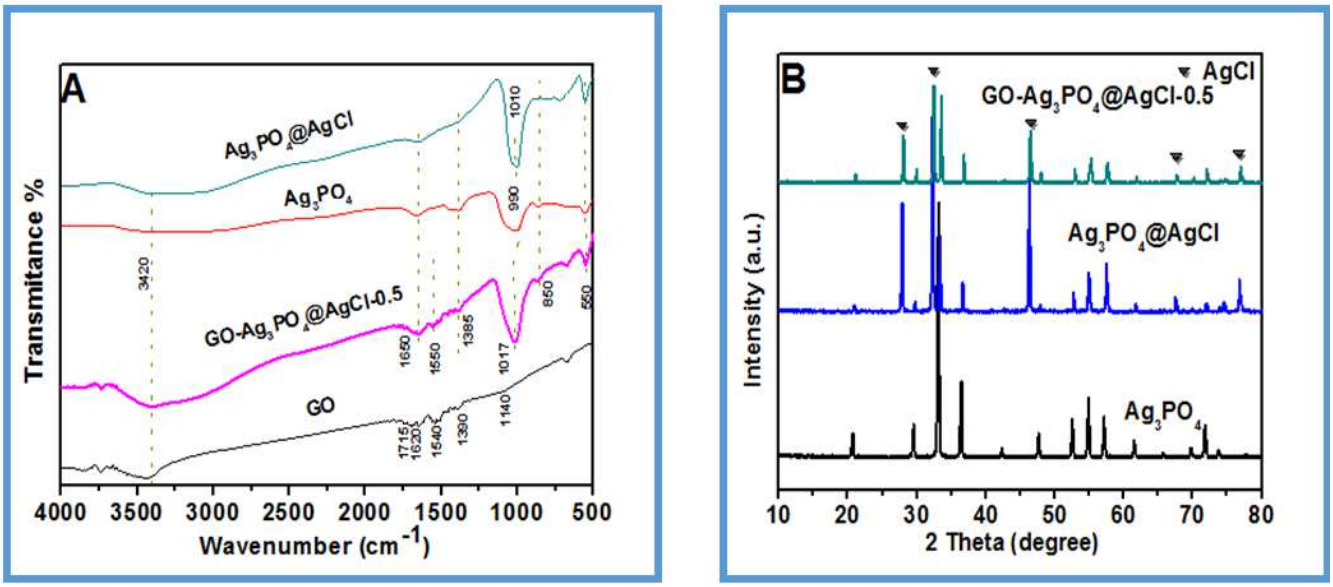

Figure 1. *(A) FTIR spectrum of the synthesized photocatalysts. (B) XRD patterns of the synthesized photocatalyst*

3.3. SEM Analysis

The morphology and structure of the synthesized samples are also characterized by field-emission scanning electron microscopy (SEM). It can be seen in Figure 2(A) that, Ag_3PO_4 possess an irregular sphere-like polyhedral morphology with an average diameter of 650 nm. As shown in Figure 2(B), it is

clearly seen that, AgCl is grown on the surface of Ag_3PO_4 to form Ag_3PO_4@AgCl composite with heterogeneous structure with average diameters less than that of Ag_3PO_4 due to the interaction between two species. As in the SEM images in Figure 2(C), after the interaction between GO and Ag^+ followed by the addition of PO_4^{3-} and Cl^- into this synthesis system, GO-Ag_3PO_4@AgCl-0.5 composites is obtained; in this process, first, the electrostatic properties drive the self-assembly of the positively charged Ag^+ and the negatively charged GO sheets, then, the Ag_3PO_4 particles are generated on the surface of GO sheets after the addition of PO_4^{3-}, afterward, AgCl particles are epitaxially grown on the surface of Ag_3PO_4, resulting on a large amount of Ag_3PO_4@AgCl-0.5 particles distributed on the surface of the flexible GO sheets. SEM observations imply that the presence of GO has a luminous effect on the morphology of Ag_3PO_4@AgCl-0.5 particles. As a result, the specific surface area is decreased, which might be a key reason for the enhanced photocatalytic activity [32]. Moreover, the smaller size Ag_3PO_4@AgCl of GO-Ag_3PO_4@AgCl-0.5 composites might supply enough contact surface area between the GO sheets and Ag_3PO_4@AgCl particles which support the charge-carrier transport, contributing partially to the higher photocatalytic performance of the GO-Ag_3PO_4@AgCl-0.5 composites [33].

3.4. TEM Analysis

Figure 2(D, E, and F) shows the TEM image of GO-Ag_3PO_4@AgCl-0.5, Ag_3PO_4@AgCl and Ag_3PO_4 respectively. As seen clearly, all the results are in good agreement with that of SEM image. As a result, GO-Ag_3PO_4@AgCl-0.5 composite is successfully fabricated with Ag_3PO_4@AgCl-0.5 particle size less than that of Ag_3PO_4@AgCl, contributing to the best photocatalytic activity of GO-Ag_3PO_4@AgCl-0.5 which would be discussed latter.

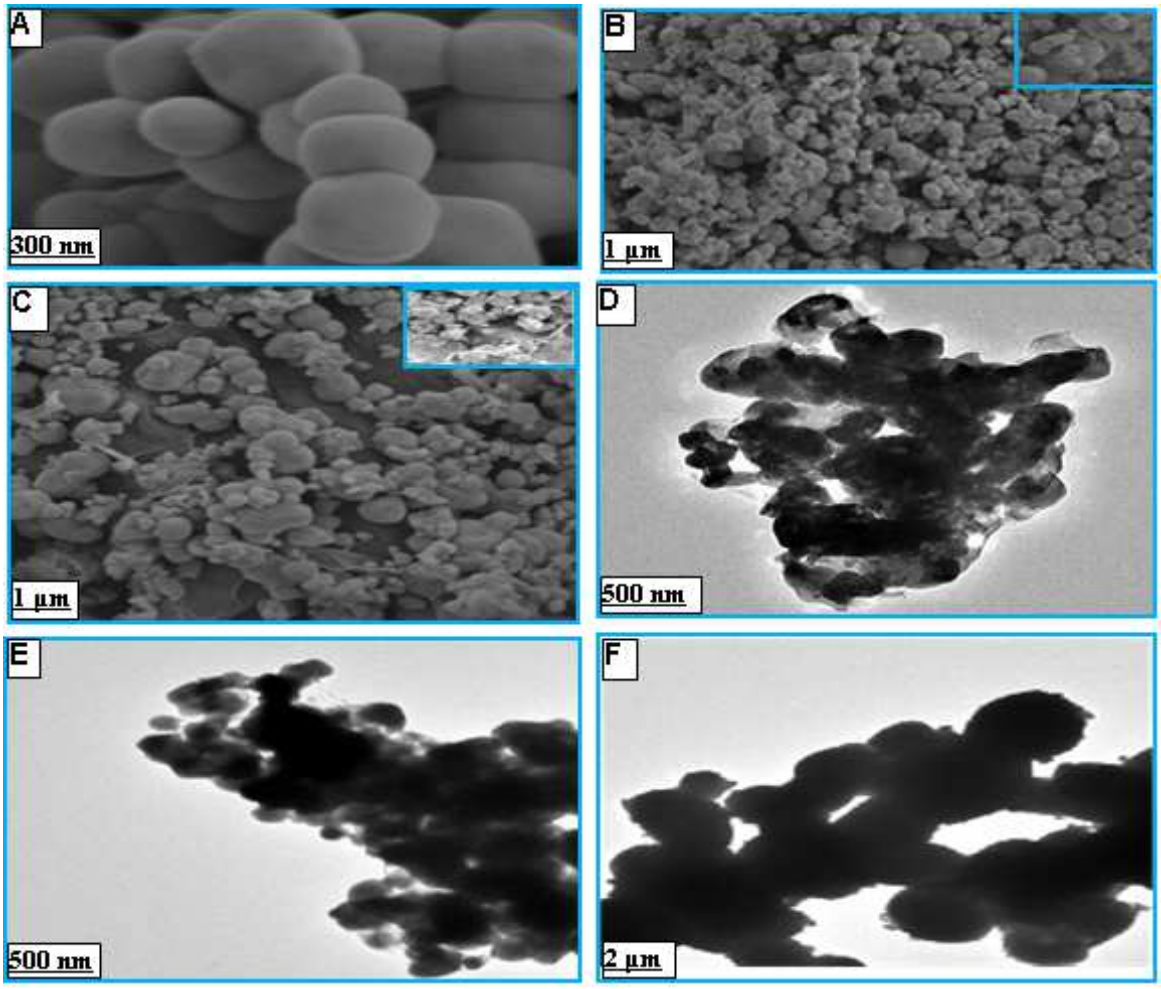

Figure 2. *SEM images of (A) Ag_3PO_4 (B) Ag_3PO_4@AgCl (C) GO-Ag_3PO_4@AgCl-0.5. And TEM images of (D) GO-Ag_3PO_4@AgCl-0.5, (E) Ag_3PO_4@AgCl and (F) Ag_3PO_4.*

3.5. XPS Analysis

The chemical composition and the valence state of the different species are determined by XPS measurements. The peak positions in all of the XPS spectra are calibrated with C 1s at 284.6 eV. Figure 3(A) shows the XPS spectrum of GO-Ag_3PO_4@AgCl-0.5, as seen, the survey contains carbon, oxygen, phosphorous, silver and chloride elements. The XPS peaks of Ag 3d are shown in Figure 3(B) the peak at 367.5 and 373.5 eV are attributed to Ag $3d_{5/2}$ and Ag $3d_{3/2}$ respectively,

confirming the presence of Ag^+ on the as-prepared composite [34]. As in Figure 3(C) the peaks with binding energies 184.6, 186.1 and 188.1 eV are corresponded to the following functional groups C-C in aromatic rings, C-O of epoxy and alkoxy groups and O-C=O of the carbonyl group, respectively [35]. The high resolution XPS spectrum in Figure 3(D) shows the peaks with binding energies of 530.6 and 532.6 eV which are assigned to the O 1s peaks, which correspond to the oxygen element of the Ag_3PO_4 crystal lattice and the hydroxyl or carboxyl groups on the surface of GO [36]. As in Figure 3(E) the Cl 2p is deconvoluted into two peaks at 197.5 and 199.1 eV [37]. P 2p spectra shows peak at 133.3 eV as in Figure 3(F), which may attributed to the P^{5+} in PO_4^{3-} [34]. The XPS results further confirmed that the GO-Ag_3PO_4@AgCl-0.5 is successfully fabricated.

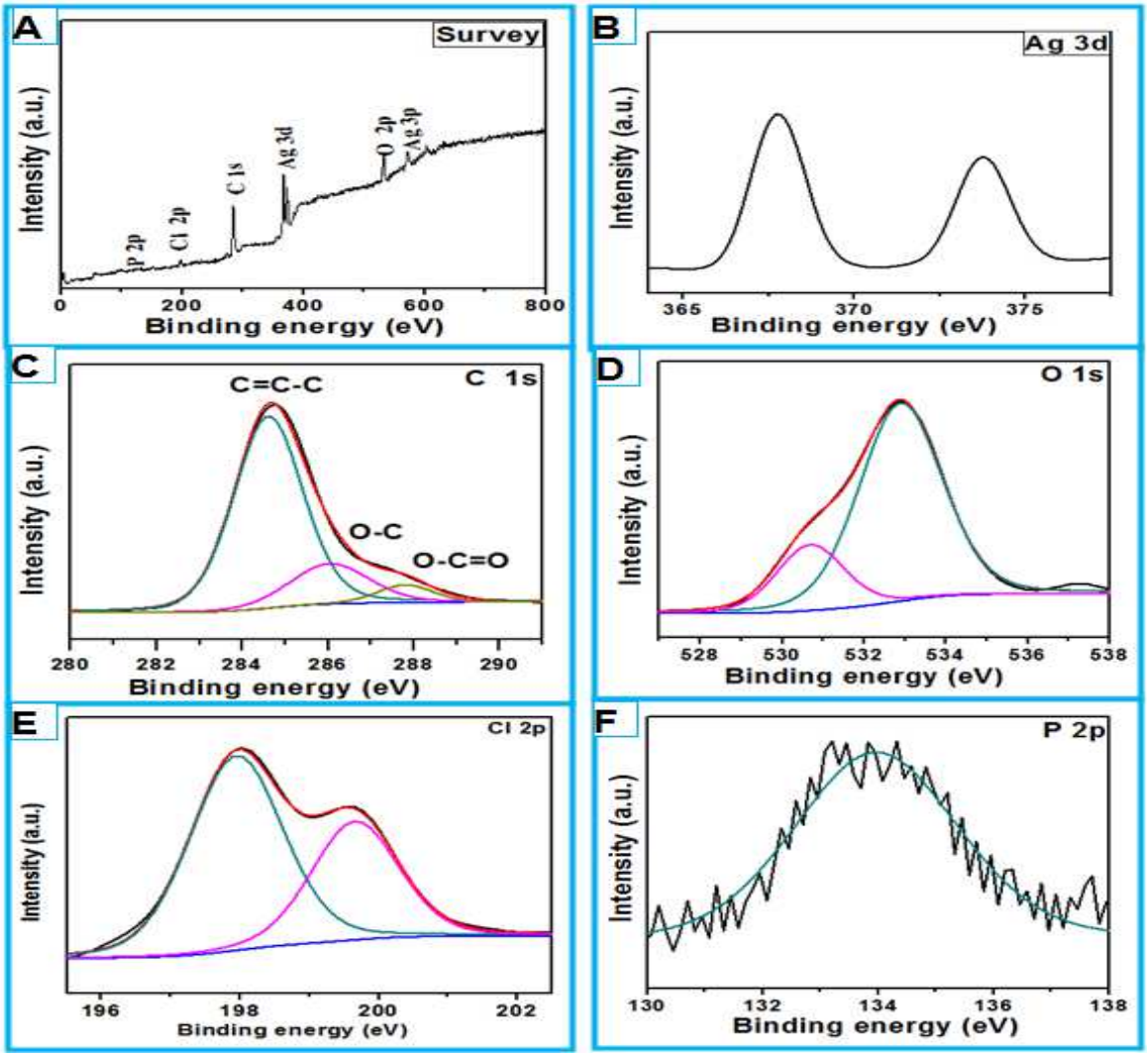

Figure 3. *XPS spectra of the GO- Ag_3PO_4@AgCl-0.5 composite: (A) XPS survey spectrum, (B) high-resolution Ag 3d spectrum, (C) high-resolution C 1s spectra, (d) high-resolution O 1s spectrum, (E) high-resolution Cl 2p spectrum, (F) high-resolution P 2p spectrum.*

3.6. UV-Vis Diffuse Reflectance Spectra Analysis

UV-Vis diffuse reflectance measurements of Ag_3PO_4, Ag_3PO_4@AgCl and GO-Ag_3PO_4@AgCl-0.5 composites are shown in Figure 4(A), it can be seen clearly that Ag_3PO_4 can absorb visible light around 530 nm [38]. In the GO-Ag_3PO_4@AgCl-0.5 composite spectra small shift in the band edge position is observed compared with pure Ag_3PO_4 and Ag_3PO_4@AgCl, moreover the absorbance higher than 500 nm is enhanced. Suggesting that GO-Ag_3PO_4@AgCl-0.5 photocatalyst may has higher efficiency to absorb visible light. In addition, the recombination rate of the electron–hole pair is successfully reduced.

3.7. PL Spectra Analysis

The transfer and recombination processes of the photogenerated electron–hole pairs can be detected by the PL spectra of the synthesized photocatalysts. The lower PL intensity is the less recombination rate of the photogenerated charge carriers [39]. Thus the better photocatalytic activity in the photocatalytic reaction. As in Figure 4(B), the PL spectra of GO-Ag_3PO_4@AgCl-0.5 and Ag_3PO_4@AgCl are show strong peak around 400 nm which attributed to charge recombination of O 2p orbitals and d orbital of Ag^+ for Ag_3PO_4 [25] and weak peak at 530 nm is attributed to Ag_3PO_4.

Peak at around 474 nm is assigned to AgCl. The graphene-based photocatalyst is exhibited lower peak intensity of PL spectra than that of Ag_3PO_4@AgCl, indicating that the migration of the photogenerated species between AgCl, Ag_3PO_4 and graphene sheets. Thus, confirming the effectiveness of the GO-Ag_3PO_4@AgCl-0.5 composite for the separation of the photogenerated electron-hole pairs.

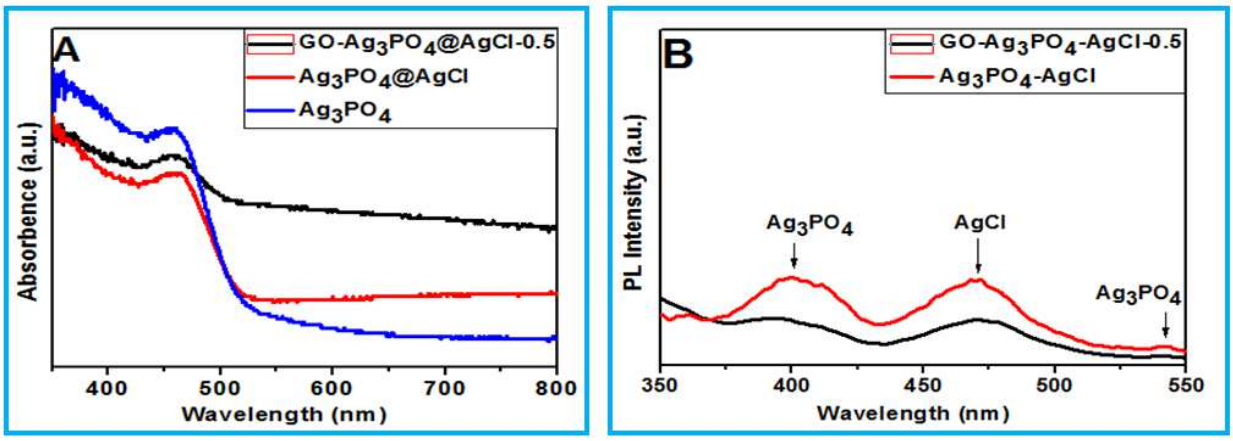

Figure 4. *(A) UV−vis diffuse reflectance spectra of GO-Ag_3PO_4@AgCl-0.5, Ag_3PO_4@AgCl and Ag_3PO_4 photocatalysts, (B) PL spectrum of the GO-Ag_3PO_4@AgCl-0.5 and Ag_3PO_4@AgCl photocatalysts.*

3.8. Study of Photocatalytic Activity

For the evaluation of the photocatalytic performance of the synthesized composites for the degradation of organic dyes under simulated sunlight, RhB is used as representative sample. Different GO-Ag_3PO_4@AgCl composites with different AgCl contents are used for the degradation of RhB under simulated sunlight irradiation to investigate the optimal Cl/P molar ratio in the photocatalytic process. The results reveal that GO-Ag_3PO_4@AgCl-0.5 is presented the highest photocatalytic performance (Figure 5). As the Cl/P ratio increased from 0.5 to 0.7, a decrease on the photocatalytic activity of GO-Ag_3PO_4@AgCl is observed. This may be due to more AgCl particles are formed on the surface of Ag_3PO_4 which decrease the light absorbed by Ag_3PO_4. Moreover, the dye may have been isolated from the direct contact with the surface of Ag_3PO_4.

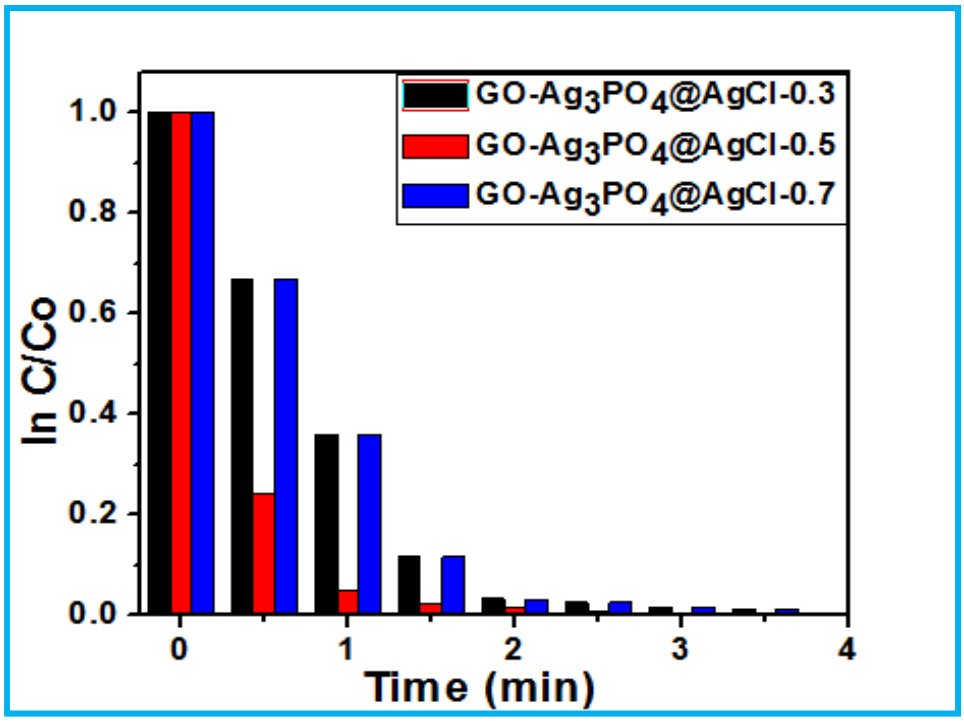

Figure 5. *Absorption changes of RhB solution under simulated sunlight irradiation in the presence of GO-Ag_3PO_4@AgCl-0.3, GO-Ag_3PO_4@AgCl-0.5 and GO-Ag_3PO_4@AgCl-0.7.*

Figure 6 shows the Photodegradation of RhB as a function of irradiation time over different photocatalysts under

simulated sunlight. The photodegradation of the RhB under light irradiation in the absence of any of the photocatalysts and in the dark condition (RhB and photocatalyst without light irradiation) is neglected. All the synthesized photocatalysts exhibited excellent photocatalytic activities toward the degradation of RhB. Among them, GO-Ag_3PO_4@AgCl-0.5 is exhibited the highest photocatalytic activity than the other photocatalysts near by 100% in 1.5 min. Ag_3PO_4@AgCl and Ag_3PO_4 are needed 3 min to exhibit degradation efficiency nearly 100% and 80% respectively. The enhanced photocatalytic activity is due to the efficient charge separation in GO-Ag_3PO_4@AgCl-0.5 catalyst system.

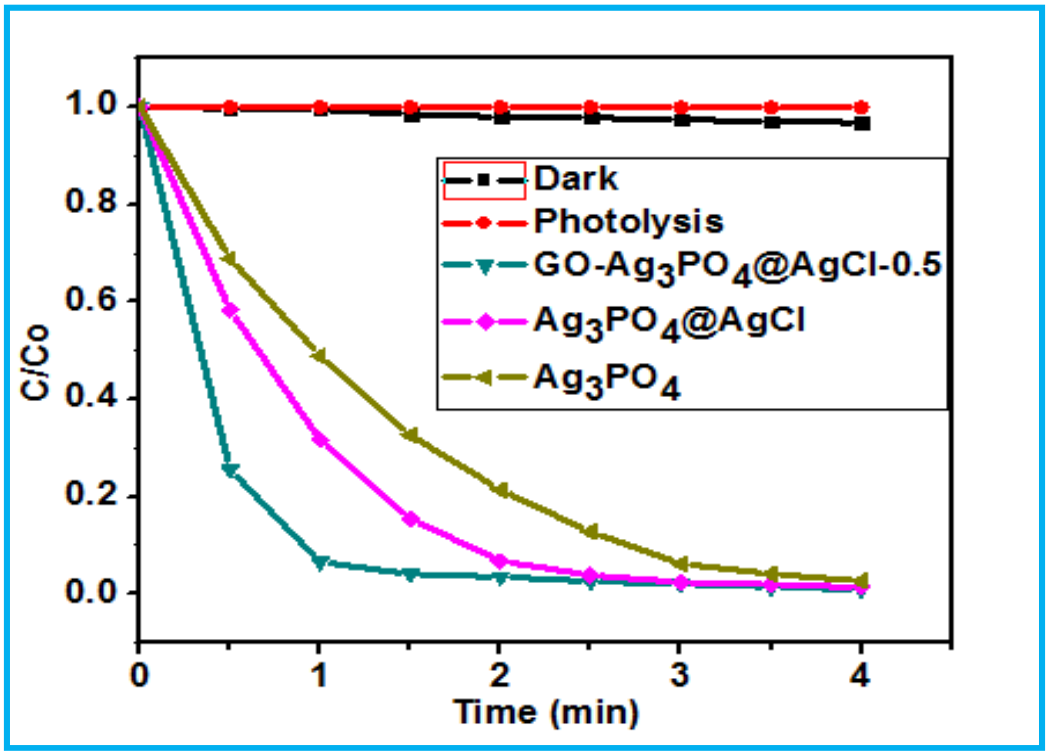

Figure 6. *Comparison of photocatalytic activity of synthesized photocatalysts for degradation of RhB under simulated sunlight irradiation.*

3.9. Kinetic Study

In order to investigate the kinetic behavior of the synthesized photocatalysts on the degradation of RhB under simulated sunlight irradiation, ln(C/Co) for RhB is plotted versus irradiation time according to the following first-order kinetic model:

$$\ln(C/Co) = -kt \quad (1)$$

Where k is the degradation rate constant, Co and C the initial concentration and the concentration at different irradiation time t of the organic dye respectively. From the result presented in Figure 7, the disappearance of RhB over the different synthesized photocatalysts under simulated sunlight irradiation is shown to fit a pseudo first order kinetics pattern, with R^2 of 0.9849, 0.9683 and 0.9845 for GO-Ag_3PO_4@AgCl-0.5, Ag_3PO_4@AgCl and Ag_3PO_4 respectively, and degradation rate constants of 2.062, 1.091 and 0.8855 min^{-1} for GO-Ag_3PO_4@AgCl-0.5, Ag_3PO_4@AgCl and Ag_3PO_4 respectively. From the values of k_{obs} and R^2 shown in Table l, it is concluded that the degradation of RhB over the as-synthesized GO-Ag_3PO_4@AgCl-0.5 under simulated sunlight irradiation is faster than that over Ag_3PO_4@AgCl and Ag_3PO_4, confirming that GO has effectively enhanced the charge separation in the GO-Ag_3PO_4@AgCl-0.5 composite compared with Ag_3PO_4@AgCl.

Table 1. *Degradation rate constants of RhB over the different synthesized photocatalysts under simulated sunlight irradiation.*

Photocatalysis	k_{obs}	R^2
GO-Ag_3PO_4@AgCl-0.5	2.062	0.9849
Ag_3PO_4@AgCl	1.091	0.9683
Ag_3PO_4	0.8855	0.9845

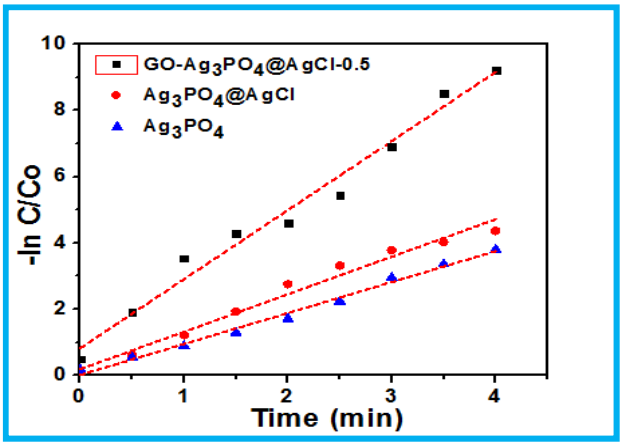

Figure 7. *Comparison of photocatalytic activity of synthesized photocatalysts for degradation of RhB.*

3.10. Stability Study

The stability and recyclability of GO-Ag_3PO_4@AgCl-0.5 are evaluated by additional experiments to degrade RhB under simulated sunlight irradiation cycled for three times [Figure 8(A)]. It can be observed that GO-Ag_3PO_4@AgCl-0.5 have good stability for the degradation of RhB under sunlight irradiation during three cycles.

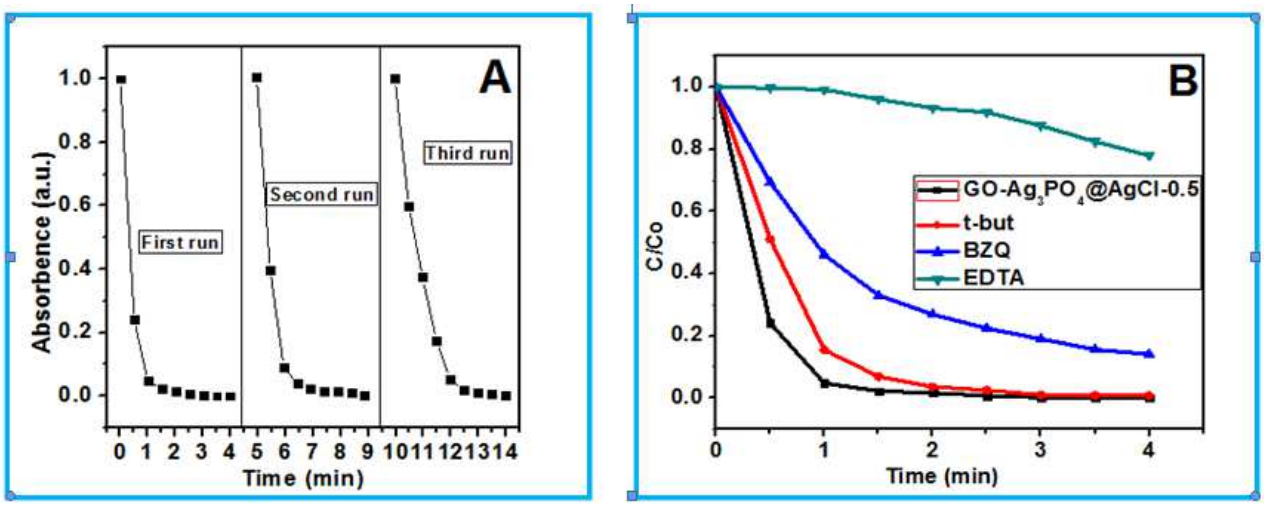

Figure 8. *(A) Stability study on the photocatalytic degradation of RhB solution over GO-Ag_3PO_4@AgCl-0.5 composite under simulated sunlight irradiation, and (B) Effect of reactive species on the photocatalytic degradation process of RhB solution over GO-Ag_3PO_4@AgCl-0.5.*

3.11. Photocatalytic Mechanism

To investigate the reactive oxygen species in the photocatalytic degradation process, in this study the expected active species such as h^+, $^{\bullet}OH$ or $^{\bullet}O_2^-$ effects on the photocatalytic process is examined by using BZQ as $^{\bullet}O_2^-$ scavenger, Na_2-EDTA as h^+ scavenger and tert-butanol as $^{\bullet}OH$ scavenger. The experimental results [Figure 8(B)] have indicated that the addition of BZQ to the photocatalytic system has decreased the photocatalytic activity of GO-Ag_3PO_4@AgCl-0.5 for the degradation of RhB in 1.5 min from 100% to 60%, indicating that $^{\bullet}O_2^-$ radicals have affected the degradation process. The addition of Na_2-EDTA has caused the highest deactivation of GO-Ag_3PO_4@AgCl-0.5 which has given a referring to; EDTA ions may act as capture or electrons donor, indicating that the holes have played the major role on the degradation of RhB. Besides, the presence of tert-butanol has negligible effect on the photocatalytic activity, suggesting that the $^{\bullet}OH$ radicals do not play a key role in the degradation process.

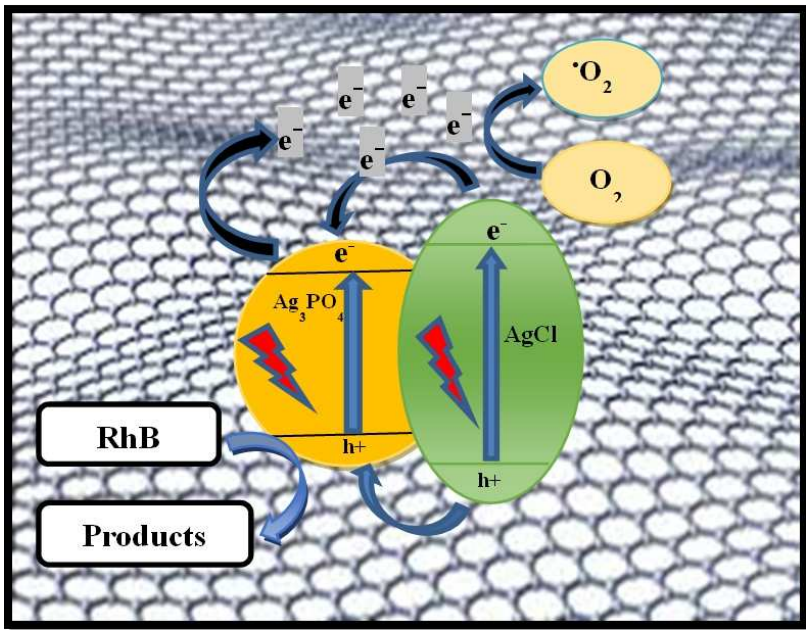

Figure 9. *Proposed mechanism of enhanced photocatalytic activity for the GO-Ag_3PO_4@ AgCl.*

Based on the above results, the reaction mechanism can be proposed as seen in Figure 9, when GO-Ag_3PO_4@AgCl-0.5

composite is exposed to simulated sunlight the electrons in the valence band of AgCl could transfer to its conductive band (CB) leaving holes behind, then transfer to the CB of Ag_3PO_4, afterwards, the photogenerated electrons on the conductive band of Ag_3PO_4 could efficiently transfer to the GO sheets, thus enhance the charge separation on the surface of Ag_3PO_4, resulting on the improvement of the photocatalytic activity. The electrons on the GO reduce the molecular oxygen to form super-oxide radicals $^{\bullet}O_2^-$ which further degrade RhB. On the other hand, the holes on the valence band (VB) of AgCl could transfer to the VB of Ag_3PO_4. As reported previously [34], the photogenerated holes on Ag_3PO_4 could not oxidize H_2O into $^{\bullet}OH$ radicals. Because the valence band edge potential of Ag_3PO_4 (2.64 V) is less positive than the standard redox potential of $^{\bullet}OH/H_2O$ (2.72 V) [40,41]. Thus the photogenerated holes on the VB of Ag_3PO_4 could directly react with RhB.

From the results of FT-IR, XRD, SEM, XPS, UV-Vis diffuse reflectance, PL and the photocatalytic degradation process mentioned above, the enhancement of the photocatalytic activity of GO-Ag_3PO_4@AgCl-0.5 over Ag_3PO_4@AgCl may be due to the efficiency of GO for the separation and transformation of the photogenerated electron-hole pairs. Also, GO is become a p-type semiconductor because of possessing a large amount of oxygen bonding on the sp^3 hybridized carbon, so, its conduction band is the antibonding π^* orbital and the O 2p orbital its valence band [42]. Thus a p/n heterojunction can be form when GO is combined with Ag_3PO_4 (n-type semiconductor), resulting on more efficient charge separation. Moreover, the electrostatic interaction between the negatively charged GO and positively charged RhB let the cationic dye to concentrate on the surface of the GO sheets, thus accelerate the interaction between the photogenerated species and the RhB, which promote the degradation process [43].

4. Conclusion

In summary, a GO-Ag_3PO_4@AgCl composite with high simulated sunlight photocatalytic performance was successfully prepared through a facile, environmentally friendly, and economical in-situ ion-exchange method. GO-Ag_3PO_4@AgCl-0.5 exhibited the highest photocatalytic activity for the degradation of RhB under simulated sunlight irradiation compared with Ag_3PO_4@AgCl and pure Ag_3PO_4. GO sheets with excellent electron accepting and transporting properties effectively enhanced the photocatalytic activity of Ag_3PO_4@AgCl. Moreover, the photocatalytic mechanism investigations demonstrated that h^+ and $^{\bullet}O_2^-$ played a key role in the degradation of RhB over GO-Ag_3PO_4@AgCl-0.5 composite under simulated sunlight irradiation. The disappearance of the RhB was showed to fit a pseudo first order kinetic pattern. The resulting GO-Ag_3PO_4@AgCl-0.5 composite may be a promising efficient photocatalyst for the degradation of organic pollutants in the industrial and engineering field.

Acknowledgments

This work was supported by the Natural Science Foundation of China (Grant Nos. 21327005, 21175108); the Program for Chang Jiang Scholars and Innovative Research. Team, Ministry of Education, China. (Grant No. IRT1 283); the Program for Innovative Research Group of Gansu Province, China (Grant No. 1210RJIA001).

References

[1] Kubacka, M.F. Garcia, G. Colon, Chemical Reviews, 2012, 112, 1555-1614.

[2] H. Tong, S.X. Ouyang, Y.P. Bi, N. Umezawa, M. Oshikiri, J. Ye, Advanced Materials, 2012, 24, 229-251.

[3] Ratna1, B.S. Padhi, Environmental Sciences, 2012, 3, 940-955.

[4] Y.P. Bi, S.X. Ouyang, N. Umezawa, J.Y. Cao, J. H. Ye, American Chemical Society, 2011, 133, 6490-6492.

[5] Y.P. Bi, H.Y. Hu, S.X. Ouyang, G.X. Lu, J.Y. Cao, J.H. Ye, Chemical Communications, 2012, 48, 3748-3750.

[6] W.G. Wang, B. Cheng, J.G. Yu, G. Liu, W.H. Fan, Chemistry – An Asian J., 2012, 7, 1902-1908.

[7] H. Wang, L. He, L.H. Wang, P.F. Hu, L. Guo, X.D. Han, J.H. Li, CrystEngComm, 2014, 14, 8342-8344.

[8] K. Santosh, T. Surendar, B. Arabind, S. Vishnu, Materials Chemistry A, 2013, 1, 5333-5340.

[9] Y. P. Bi, H. Y.Hu, S.X. Ouyang, Z.B. Jiao, G.X. Lu, J.H. Ye, Chemistry - A European J., 2012, 18, 14272-14275.

[10] W.F. Yao, B. Zhang, C.P. Huang, C. Ma, X.L. Song, Q.J. Xu, Materials Chemistry, 2012, 22, 4050-4055.

[11] W. Liu, M. L. Wang, C.X. Xu, S.F. Chen, X.L. Fu, Materials Research Bulletin, 2013, 48, 106-113.

[12] L.L. Zhang, H.C. Zhang, H. Huang, Y. Liu, Z.H. Kang, Chemistry, 2012, 36 1541-1544.

[13] Y. Bi, S. Ouyang, J. Cao, J. Ye, Physical Chemistry Chemical Physics, 2011, 13, 10071-10075.

[14] Q. J. Xiang, J.G. Yu, M. Jaroniec, Chemical Society Reviews, 2012, 41, 782-796.

[15] X.Q. An, J.C. Yu, RSC Advances, 2011, 1, 1426-1434.

[16] B.J. Jiang, C.G. Tiang, Q.J. Pan, Z. Jiang, J.Q. Wang, W.S. Yan, H.G. Fu, Physical Chemistry C, 2011, 115, 23718-23725.

[17] H. Zhang, X.F. Fan, X. Quan, S. Chen, H.T. Yu, Environmental Science and Technology, 2011, 45, 5731-5736.

[18] G.D. Chen, M. Sun, Q. Wei, Y.F. Zhang, B.C. Zhu, B. Du, Hazardous Material, 2013, 244, 86-93.

[19] A. Yanhui, W. Peifang, W. Chao, H. Jun, Q. Jin, Applied Surface Science, 2013, 271, 265-270.

[20] H. Guangyu, Q. Maogong, S. Xiaoqiang, C. Qun, W. Xin, C. Haiqun, Powder Technology, 2013, 246, 278-283.

[21] B.J. Jiang, Y.H. Wang, J.Q. Wang, C.G. Tiang, W.J. Li, Q.M. Feng, Q.J. Pan, H.G. Fu, ChemCatChem, 2013, 5, 1359-1367.

[22] W.S. Hummers, R.E. Offeman, American Chemical Society, 1958, 80, 1339-1339.

[23] M.C. Yin, Z.S. Li, J.H. Kou, Z.G. Zou, Environmental Science and Technology, 2009, 43 8361-8366.

[24] P.Y. Dong, Y.H. Wang, B.C. Cao, S.Y. Xin, L.N. Guo, J. Zhang, F. H. Li, Applied Catalysis B, 2013, 132, 45-53.

[25] Q.H. Liang, Y. Shi, W.J. Ma, Z. Li, X.M. Yang, Physical Chemistry, Chemical Physics, 2012, 14, 15657-15665.

[26] H. Tang, K. Prasad, R. Sanjinès, P.E. Schmid, F. Lévy, Applied Physics, 1994, 75, 2042-2047.

[27] H.N. Ng, C. Calvo, R. Faggiani, Acta Crystallographica Section B: Structural Science, 1978, 34, 898-899.

[28] A. Pongsaton, S. Sumetha, Advanced Powder Technology, 2014, 25, 1026-1030.

[29] V. Gopinath, S. Priyadarshini, N.M. Priyadharsshini, K. Pandian, P. Velusamy, Materials Letters, 2013, 91, 224-227.

[30] X.F. Yang, H.Y. Cui, Y. Li, J.L. Qin, R.X. Zhang, H. Tang, American Chemical Society Catalysis, 2013, 3, 363-369.

[31] J. Liu, H. Bai, Y. Wang, Z. Liu, X. Zhang, D.D. Sun, Advanced Functional Materials, 2010, 20, 4175-4181.

[32] X. Gu, Sh.Zhang, B. Wang, Y. Qiang, Optoelectronics Letters, 2014, 10, 219-222.

[33] M. Zhu, P. Chen, M. Liu, American Chemical Society Nano, 2011, 5, 4529-4536.

[34] M. Ge, N. Zhu, Y.P. Zhao, J. Li, L. Liu, Industrial & Engineering Chemistry Research, 2012, 51, 5167-5173.

[35] W.G. Wang, J.G. Yu, Q.J. Xiang, B. Cheng, Applied Catalysis B, 2012, 119, 109-116.

[36] Z. Hu, Y.D. Huang, S.F. Sun, W.C. Guan, Y.H. Yao, P.Y. Tang, C. Li, Carbon, 2012, 50, 994-1004.

[37] M. Zhu, P. Chen, M. Liu, Material Chemistry, 2011, 21, 16413-16419.

[38] A.V. Murugan, T. Muraliganth, A. Manthiram, Chemistry of Materials, 2009, 21, 5004-5006.

[39] Z.G. Yi, N. Kikugawa, T. Kako, H. Stuart-Williams, H. Yang, J.Y. Cao, W. J. Luo, Z.S. Li, Y. Liu, R.L. Withers, Nature Materials, 2010, 9, 559-564.

[40] X.G. Ma, B. Lu, D. Li, R. Shi, C.S. Pan, Y.F. Zhu, Physical Chemistry C, 2011, 115, 4680-4687.

[41] J.Cao, B.D. Luo, H.L. Lin, B.Y. Xu, S.F. Chen, Hazardous Material, 2012, 217, 107-115.

[42] T.F. Yeh, J.M. Syu, C. Cheng, T.H. Chang, H.S. Teng, Advanced Functional Material, 2010, 20, 2255-2262.

[43] S. Bai, X. Shen, H. Lv, G. Zhu, C. Bao, Y. Shan, Colloid and Interface Science, 2013, 405, 1-9.